JOURNAL OF GUIDANCE, CONTROL, AND DYNAMICS
Vol. 30, No. 1, January–February 2007

Minimum Angular-Impulse Control for a Large Flexible Spacecraft

E. M. Cliff* and T. L. Herdman†
Virginia Polytechnic Institute and State University, Blacksburg, Virginia 24061
and
Z. Y. Liu‡
University of Minnesota, Duluth, Minnesota 55812

DOI: 10.2514/1.24275

Characterization and implementation of efficient rotational motions of flexible spacecraft have been of research interest for more than 20 years. In the present study we consider rest-to-rest pointing maneuvers for a very large spacecraft, so that limits on available angular momentum are paramount. A formal system of differential equations is developed based on a model that includes a rigid central hub and Euler–Bernoulli appendages. The model is recast in an appropriate state-space and standard functional analysis methods are used to prove well-posedness and to establish a framework for numerical approximation. Several variants of minimum-angular moment problems are studied; ultimately, we focus on a low-dimensional control parameterization based on a family of versine functions and on quasi-static structural response. Results are characterized in terms of simple formulas and sensitivity with respect to problem data is presented.

I. Introduction

THE Innovative Space-based Radar Antenna Technology program (ISAT) is a Defense Advanced Research Projects Agency/Special Projects Office initiative to develop a large aperture radar for persistent ground surveillance. Our analysis is based on a 300 m long, government reference design.[§] At this scale, shape distortion will be an important issue. Traversing among surveillance regions may require slewing of the spacecraft, whereas successful operation of the radar imposes distortion limits.

In this study, we consider the rotational motions of a spacecraft consisting of a rigid-hub of diameter $2a$ with two flexible (beam) appendages, each of length L (see Fig. 1). In this figure, $\hat{i}_b$ and $\hat{j}_b$ are body-fixed axes, orthogonal to the axis of rotation; in the undeformed state, the beams lie along the $\pm\hat{i}_b$ axis. Whereas the beams are constructed from truss elements, here we focus on an equivalent Euler–Bernoulli beam model.

Time-efficient rotational maneuvers for flexible spacecraft have been studied by many authors [1–9]. For the case of a rigid-body with a bound on the applied torque (say $|M(t)| \le \tilde{M}$), time-optimal control is bang–bang, with a single-switch at midmaneuver. Simple calculations reveal that the maneuver time is given by

$$t_f = 2\sqrt{\frac{I_o\theta_f}{\tilde{M}}}$$

where I_o is the moment of inertia, and θ_f is the prescribed rotation angle. The angular momentum required from an internal device is given by

$$h = \frac{\tilde{M}t_f}{2} = \sqrt{I_o\tilde{M}\theta_f} = \frac{2I_o\theta_f}{t_f}$$

This amount of angular momentum is required for the spin-up phase of the maneuver and can be returned to an internal momentum storage device in the stopping phase. For ISAT $I_o \approx 28 \times 10^6$ kg · m^2, and several values of maneuver-time and stored momentum required for a 90 deg maneuver are shown in Table 1.

In the presence of flexibility, strictly time-optimal maneuvers add a pair of control switches for each mode; these are placed symmetrically about the midpoint (no damping). The switch pairs are nested (higher frequency modes are closer to the midpoint [1,3]) and, in the limit, the control *chatters* at the midpoint. Because real controls cannot switch instantly, it has long been appreciated that practical implementation requires some adaptation [8]. This has led to various control smoothing strategies and so-called near minimum-time maneuvers [4–6,8,9]

Various linear-quadratic designs, including minimum-effort control [10], have also been studied [11,12]. In particular, minimum-effort control of the rigid-body implies that the applied moment is an affine function of time, specifically, $M(t) = \tilde{M}[1 - (2t/t_f)]$. Solution of the second order boundary-value problem characterizing rest-to-rest rotation through θ_f leads to

$$\tilde{M} = \frac{6I_o\theta_f}{t_f^2} \quad \text{and} \quad h = \frac{\tilde{M}t_f}{4} = \frac{3I_o\theta_f}{2t_f}$$

Sample results for the minimum-effort maneuver are shown in Table 2. Note that whereas the required maneuver time increases (as expected), the required angular momentum decreases. Because the momenta are still rather large, the natural question is "What is the minimum required momentum?"

Note that using thrust control, the minimum-fuel problem has some connection to the minimum angular-momentum problem. Carter et al. [5] study a minimum-fuel problem for attitude control of the Advanced Space Structures Technology Research Experiment test bed [13]. However, experimental difficulties led to a modified cost-functional which blurs the connection to the minimum angular-momentum problem considered here.

Presented as Paper 1979 at the Gossamer Spacecraft, Newport, RI, 1–4 May 2006; received 27 March 2006; revision received 1 August 2006; accepted for publication 8 August 2006.

*Professor Emeritus, Interdisciplinary Center for Applied Mathematics, Associate Fellow.
†Professor, Interdisciplinary Center for Applied Mathematics.
‡Professor, Department of Mathematics.

§M. Mikulas, briefing slides & personal communications, Oct. 2004.

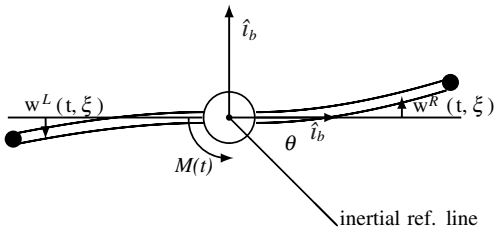

Fig. 1 System configuration.

II. Formal Model

We develop a dynamic model by decomposing the system into five components: the hub, left/right beams, and left/right tip masses. The partial differential equations describing motions of the Euler–Bernoulli beams are [1]

$$\sigma\Big[w^R_{tt}(t,\xi) + (a+\xi)\dot{\omega}(t)\Big] + \Big[EIw^R_{\xi\xi}(t,\xi)\Big]_{\xi\xi} = 0 \tag{1}$$

$$\sigma\Big[w^L_{tt}(t,\xi) + (a+\xi)\dot{\omega}(t)\Big] + \Big[EIw^L_{\xi\xi}(t,\xi)\Big]_{\xi\xi} = 0 \tag{2}$$

Here, $\sigma > 0$ is the lineal density of the beam, $\xi = 0$ corresponds to the beam–hub junction, and $\xi = L$ corresponds to the beam–tip junction. The variable ω is the angular velocity of the hub [so that $\dot{\theta}(t) = \omega(t)$]; the nonstandard acceleration terms $[(a+\xi)\dot{\omega}(t)]$ in Eqs. (1) and (2) arise from the fact that $w(t,\xi)$ is the displacement relative to a noninertial, body-fixed frame. The (ordinary differential) equations of motion for the tip masses and the hub are

$$m\dot{v}^R(t) = T^R(t) - \Big[EIw^R_{\xi\xi\xi}(t,L)\Big] \tag{3}$$

$$m\dot{v}^L(t) = T^L(t) - \Big[EIw^L_{\xi\xi\xi}(t,L)\Big] \tag{4}$$

$$\begin{aligned} I_h\dot{\omega}(t) = {} & \Big[EIw^R_{\xi\xi}(t,0)\Big] + \Big[EIw^L_{\xi\xi}(t,0)\Big] - a\Big[EIw^R_{\xi\xi\xi}(t,0)\Big] \\ & - a\Big[EIw^L_{\xi\xi\xi}(t,0)\Big] + M(t) \end{aligned} \tag{5}$$

T^R and T^L are control thrusts applied at the tips, whereas M is a control torque applied to the hub. The variable v^R (v^L) is the inertial velocity of the right (left) tip-thruster. Boundary conditions at the hub–beam interface are

$$w^k(t,0) = w^k_\xi(t,0) = 0 \qquad k = L, R \tag{6}$$

At the beam-tips, we require

Table 1 Minimum-time maneuvers, rigid-body, $\theta_f = \pi/2$

Moment, N · m	Time, min	Angular momentum, N · m/s
25	44.2	3.33×10^4
50	31.3	4.69×10^4
100	22.1	6.63×10^4
300	12.8	11.49×10^4

Table 2 Minimum-effort maneuvers, rigid-body, $\theta_f = \pi/2$

Peak moment, N · m	Time, min	Angular momentum, N · m/s
25	54.1	2.03×10^4
50	38.3	2.87×10^4
100	27.1	4.06×10^4
300	15.6	7.03×10^4

$$w^k_{\xi\xi}(t,L) = 0 \qquad k = L, R \tag{7}$$

whereas geometric compatibility at the beam-tips implies

$$v^k(t) - \Big[w^k_t(t,L) + \omega(t)(a+L)\Big] = 0 \qquad k = L, R \tag{8}$$

We shall assume that the beam properties are uniform (constant lineal mass-density σ and stiffness EI) and that the left and right beams are identical. Note that our model is linear; geometric nonlinearities (due to large deflections) and centrifugal stiffening (due to large angular rates) are not included.

III. State-Space Formulation

Our objective here is to formulate the dynamical model from Sec. II as a differential equation in an appropriate Hilbert space. Whereas one can formally apply approximation methods to the system (1–8), a state-space formulation provides a natural framework to establish existence/uniqueness, as well as convergence under numerical approximation ([14], see the Trotter–Kato theorem, p. 87 *ff*). As a first step, we eliminate v^k using Eq. (8) and write the equations as

$$\sigma\left(w^R_{tt}(t,\xi) + (a+\xi)\frac{d\omega(t)}{dt}\right) + (EI)w^R_{\xi\xi\xi\xi}(t,\xi) = 0 \tag{9}$$

$$\sigma\left(w^L_{tt}(t,\xi) + (a+\xi)\frac{d\omega(t)}{dt}\right) + (EI)w^L_{\xi\xi\xi\xi}(t,\xi) = 0 \tag{10}$$

$$m\frac{d}{dt}\Big[w^R_t(t,L) + (a+L)\omega(t)\Big] + (EI)w^R_{\xi\xi\xi}(t,L) = T^R(t) \tag{11}$$

$$m\frac{d}{dt}\Big[w^L_t(t,L) + (a+L)\omega(t)\Big] + (EI)w^L_{\xi\xi\xi}(t,L) = T^L(t) \tag{12}$$

$$\begin{aligned} I_h\frac{d\omega(t)}{dt} - (EI)\Big[w^R_{\xi\xi}(t,0) + w^L_{\xi\xi}(t,0)\Big] + a(EI)\Big[w^R_{\xi\xi\xi}(t,0) \\ + w^L_{\xi\xi\xi}(t,0)\Big] = M(t) \end{aligned} \tag{13}$$

It is helpful to use Eq. (13) to eliminate the $d\omega/dt$ terms in Eqs. (9–12), and to this end we define the boundary operator b: $H^4(0,L) \times \mathbb{R} \mapsto \mathbb{R}$ by

$$b(w,a) = w_{\xi\xi}(0) - aw_{\xi\xi\xi}(0)$$

so that Eq. (13) can be written as

$$\frac{d\omega(t)}{dt} = \frac{(EI)}{I_h}\{b[w^R(t),a] + b[w^L(t),a]\} + \frac{M(t)}{I_h} \tag{14}$$

Note that the first argument of the mapping b is in the Sobolev space $H^4(0,L)$ [15] and that b is linear in this argument. Introducing

$$v^k(t,\xi) = w^k_t(t,\xi) \quad \text{and} \quad \eta^k(t) = v^k(t,L) \qquad k = L, R$$

the (unforced) system (9–13) leads to the first-order system

$$\frac{d}{dt}\begin{bmatrix} w^R(t) \\ v^R(t) \\ w^L(t) \\ v^L(t) \\ \eta^R(t) \\ \eta^L(t) \\ \omega(t) \end{bmatrix} = \begin{bmatrix} v^R(t) \\ -\frac{(EI)}{\sigma} w^R_{\xi\xi\xi\xi}(t) - \frac{(EI)}{I_h} b[w^R(t) + w^L(t), a](a+\xi) \\ v^L \\ -\frac{(EI)}{\sigma} w^L_{\xi\xi\xi\xi}(t) - \frac{(EI)}{I_h} b[w^R(t) + w^L(t), a](a+\xi) \\ -\frac{(EI)}{m} w^R_{\xi\xi\xi}(t, L) - \frac{(EI)}{I_h} b[w^R(t) + w^L(t), a](a+L) \\ -\frac{(EI)}{m} w^L_{\xi\xi\xi}(t, L) - \frac{(EI)}{I_h} b[w^R(t) + w^L(t), a](a+L) \\ \frac{(EI)}{I_h} b[w^R(t) + w^L(t), a] \end{bmatrix} \tag{15}$$

The control inputs $[M(t), T^R(t), T^L(t)]$ give rise to an additional term

$$\mathcal{B}\begin{bmatrix} M(t) \\ T^R(t) \\ T^L(t) \end{bmatrix} \triangleq \begin{bmatrix} 0 & 0 & 0 \\ -\frac{(a+\xi)}{I_h} & 0 & 0 \\ 0 & 0 & 0 \\ -\frac{(a+\xi)}{I_h} & 0 & 0 \\ -\frac{(a+L)}{I_h} & \frac{1}{m} & 0 \\ -\frac{(a+L)}{I_h} & 0 & \frac{1}{m} \\ \frac{1}{I_h} & 0 & 0 \end{bmatrix} \begin{bmatrix} M(t) \\ T^R(t) \\ T^L(t) \end{bmatrix} \tag{16}$$

Equations (15) and (16) are to be interpreted as an abstract ordinary differential equation. To this end, we identify the state $z = \mathrm{col}(w^R, v^R, w^L, v^L, \eta^R, \eta^L, \omega)$ and define the Hilbert space

$$\mathcal{H} = H_0^2(0, L) \times L^2(0, L) \times H_0^2(0, L) \times L^2(0, L) \times \mathbb{R} \times \mathbb{R} \times \mathbb{R}$$

with the energy norm

$$\begin{aligned} \|z\|^2_{\mathcal{H}} &= (EI)\|w^R_{\xi\xi}\|^2 + \sigma\|v^R + (a+\xi)\omega\|^2 + (EI)\|w^L_{\xi\xi}\|^2 + \sigma\|v^L \\ &\quad + (a+\xi)\omega\|^2 + m|\eta^R + (a+L)\omega|^2 + m|\eta^L + (a+L)\omega|^2 \\ &\quad + I_h|\omega|^2 \end{aligned}$$

where $\|\cdot\|$ is the usual L^2 norm. We now define an operator $\mathcal{A}$: $\mathcal{H} \mapsto \mathcal{H}$ given by the right-hand side of Eq. (15) with domain

$$D(\mathcal{A}) = \left\{ z \in \mathcal{H} \,\middle|\, \begin{matrix} w^R, w^L \in H^4, & v^R, v^L \in H_0^2 \\ w^R_{\xi\xi}(L) = w^L_{\xi\xi}(L) = 0, & \eta^R = v^R(L), \eta^L = v^L(L) \end{matrix} \right\}$$

Theorem 1: $\mathcal{A}$ generates a C_0 semigroup of contractions $\{\mathcal{S}(t)\}_{t\geq 0}$ on the Hilbert space $\mathcal{H}$.

Proof. For any $z \in D(\mathcal{A})$, tedious but direct calculation reveals that

$$\langle \mathcal{A}z, z\rangle_{\mathcal{H}} = 0 \tag{17}$$

so that $\mathcal{A}$ is dissipative.

Next, we show that the range of $(I - \mathcal{A})$ is all of $\mathcal{H}$. For any $z_0 = \mathrm{col}(w_0^R, v_0^R, w_0^L, v_0^L, \eta_0^R, \eta_0^L, \omega_0) \in \mathcal{H}$, we solve the equation

$$(I - \mathcal{A})z = z_0$$

i.e.,

$$w^R(\xi) - v^R(\xi) = w_0^R(\xi) \tag{18}$$

$$v^R(\xi) + \frac{(EI)}{\sigma} w^R_{\xi\xi\xi\xi}(\xi) + \frac{(EI)}{I_h}(a+\xi)\left\{\left[w^R_{\xi\xi}(0) + w^L_{\xi\xi}(0)\right] - a\left[w^R_{\xi\xi\xi}(0) + w^L_{\xi\xi\xi}(0)\right]\right\} = v_0^R(\xi) \tag{19}$$

$$w^L(\xi) - v^L(\xi) = w_0^L(\xi) \tag{20}$$

$$v^L(\xi) + \frac{(EI)}{\sigma} w^L_{\xi\xi\xi\xi}(\xi) + \frac{(EI)}{I_h}(a+\xi)\left\{\left[w^R_{\xi\xi}(0) + w^L_{\xi\xi}(0)\right] - a\left[w^R_{\xi\xi\xi}(0) + w^L_{\xi\xi\xi}(0)\right]\right\} = v_0^L(\xi) \tag{21}$$

$$\eta^R - \frac{(EI)}{m} w^R_{\xi\xi\xi}(L) - \frac{(EI)(a+L)}{I_h}\left\{\left[w^R_{\xi\xi}(0) + w^L_{\xi\xi}(0)\right] - a\left[w^R_{\xi\xi\xi}(0) + w^L_{\xi\xi\xi}(0)\right]\right\} = \eta_0^R \tag{22}$$

$$\eta^L - \frac{(EI)}{m} w^L_{\xi\xi\xi}(L) - \frac{(EI)(a+L)}{I_h}\left\{\left[w^R_{\xi\xi}(0) + w^L_{\xi\xi}(0)\right] - a\left[w^R_{\xi\xi\xi}(0) + w^L_{\xi\xi\xi}(0)\right]\right\} = \eta_0^L \tag{23}$$

$$\omega - \frac{(EI)}{I_h}\left\{\left[w^R_{\xi\xi}(0) + w^L_{\xi\xi}(0)\right] - a\left[w^R_{\xi\xi\xi}(0) + w^L_{\xi\xi\xi}(0)\right]\right\} = \omega_0 \tag{24}$$

From Eqs. (18) and (20)

$$v^R(\xi) = w^R(\xi) - w_0^R(\xi), \qquad v^L(\xi) = w^L(\xi) - w_0^L(\xi)$$

Substituting, Eqs. (19) and (21–23) become

$$\begin{aligned} &w^R(\xi) + \frac{(EI)}{\sigma} w^R_{\xi\xi\xi\xi}(\xi) = v_0^R(\xi) + w_0^R(\xi) + (a+\xi)(\omega_0 - \omega) \\ &w^L(\xi) + \frac{(EI)}{\sigma} w^L_{\xi\xi\xi\xi}(\xi) = v_0^L(\xi) + w_0^L(\xi) + (a+\xi)(\omega_0 - \omega) \\ &w^R(L) - \frac{(EI)}{m} w^R_{\xi\xi\xi}(L) - \frac{(EI)(a+L)}{I_h}\left\{\left[w^R_{\xi\xi}(0) + w^L_{\xi\xi}(0)\right] - a\left[w^R_{\xi\xi\xi}(0) + w^L_{\xi\xi\xi}(0)\right]\right\} = \eta_0^R + w_0^R(L) \\ &w^L(L) - \frac{(EI)}{m} w^L_{\xi\xi\xi}(L) - \frac{(EI)(a+L)}{I_h}\left\{\left[w^R_{\xi\xi}(0) + w^L_{\xi\xi}(0)\right] - a\left[w^R_{\xi\xi\xi}(0) + w^L_{\xi\xi\xi}(0)\right]\right\} = \eta_0^L + w_0^L(L) \end{aligned}$$

The latter two equations provide two boundary conditions for the dependent variables w^R and w^L and with the additional six boundary conditions

$$w^R(0) = w^R_\xi(0) = w^L(0) = w^L_\xi(0) = w^R_{\xi\xi}(L) = w^L_{\xi\xi}(L) = 0$$

we get unique solutions

$$w^R, w^L \in H^4 \cap H_0^2$$

Thus, $v^R, v^L \in H_0^2$. Finally, we get $\eta^k = v^k(L)$, $k = R, L$ from the domain restriction and ω from Eq. (24). It follows that the range $R(I - \mathcal{A}) = \mathcal{H}$. Combining this and the fact that $\mathcal{A}$ is dissipative, Theorem 4.6 in ([14], see page 16) implies that $D(\mathcal{A})$ is dense in $\mathcal{H}$. The result then follows from the Lumer–Phillips Theorem ([14], see page 14). □

The meaning of Theorem 1 is that for any initial condition $z_o \in \mathcal{H}$, the solution of the (unforced) initial-value problem (IVP)

$$\dot{z}(t) = \mathcal{A}z(t), \qquad z(0) = z_0$$

is given by

$$\dot{z}(t) = \mathcal{S}(t)z_0$$

The semigroup $\{\mathcal{S}(t)\}_{t\geq 0}$ is the generalization of $\{e^{\mathcal{A}t}\}$ in the finite-dimensional case. The *contraction property* means that the norm of the solution is nonincreasing ($\|z(t)\| \leq \|z_0\|$). For the forced case $[u(t) \neq 0]$ one has a variation of parameters formula, analogous to

the finite-dimensional case. The utility of this approach is that it provides a straightforward way to establish well-posedness for the IVP. In more practical terms, it provides a framework for convergent numerical approximations.

IV. Symmetric and Asymmetric Motions

Before proceeding it is useful to consider that under special initial conditions and forcing the deformations of the two beams will be identical, and this observation can be used to reduce the computational burden. To this end we define *symmetric* and *asymmetric* variables by

$$w^s(t,\xi)=\frac{w^R(t,\xi)+w^L(t,\xi)}{2} \qquad w^a(t,\xi)=\frac{w^R(t,\xi)-w^L(t,\xi)}{2} \qquad v^s(t,\xi)=\frac{v^R(t,\xi)+v^L(t,\xi)}{2} \qquad v^a(t,\xi)=\frac{v^R(t,\xi)-v^L(t,\xi)}{2}$$

$$\eta^s(t)=\frac{\eta^R(t)+\eta^L(t)}{2} \qquad \eta^a(t)=\frac{\eta^R(t)-\eta^L(t)}{2} \qquad T^s(t)=\frac{T^R(t)+T^L(t)}{2} \qquad T^a(t)=\frac{T^R(t)-T^L(t)}{2}$$

The boundary conditions (6) and (7) still apply, now with $k=a,s$, whereas the geometric compatibility conditions (8) are transformed to

$$\eta^s(t)-[w^s_t(t,L)+\omega(t)(a+L)]=0, \quad \text{and} \qquad \eta^a(t)-w^a_t(t,L)=0$$

In terms of these new dependent variables, the first-order system (15) and (16) is written

$$\frac{d}{dt}\begin{bmatrix} w^a(t)\\ v^a(t)\\ \eta^a(t)\\ w^s(t)\\ v^s(t)\\ \eta^s(t)\\ \omega(t)\end{bmatrix}=\begin{bmatrix} v^a(t)\\ -\left(\frac{EI}{\sigma}\right)w^a_{\xi\xi\xi\xi}(t)\\ \left(\frac{EI}{m}\right)w^a_{\xi\xi\xi}(t,L)+\frac{T^a(t)}{m}\\ v^s(t)\\ -\left(\frac{EI}{\sigma}\right)w^s_{\xi\xi\xi\xi}(t)-\frac{(a+\xi)}{I_h}[2(EI)b(w^s,a)+M(t)]\\ \left(\frac{EI}{m}\right)w^s_{\xi\xi\xi}(t,L)-\frac{(a+L)}{I_h}[2(EI)b(w^s,a)+M(t)]+\frac{T^s(t)}{m}\\ [2(EI)b(w^s,a)+M(t)]/I_h\end{bmatrix} \tag{25}$$

It is clear that the asymmetric motion $[w^a(t),v^a(t),\eta^a(t)]$ is uncoupled from the symmetric motion $[w^s(t),v^s(t),\eta^s(t)]$ and that with zero initial data and zero forcing $[T^a(t)=0]$, the asymmetric motion is identically zero. Indeed, with $T^a(t)\neq 0$, the system in Fig. 1 would translate in the plane; such degrees of freedom are not included in the model. Thus, we consider only symmetric motions in the following. Whereas the variable ω can be recovered as a quadrature in terms of the symmetric variables, we include it in our symmetric model to account for the energy explicitly.

V. Weak Form

Define the symmetric state $z^s\triangleq \mathrm{col}(w^s,v^s,\eta^s,\omega)$ and the Hilbert space

$$\mathcal{H}^s=H^2_0(0,L)\times L^2(0,L)\times\mathbb{R}\times\mathbb{R}$$

with the energy norm

$$\|z^s\|^2_{\mathcal{H}^s}=(EI)\|w^s_{\xi\xi}\|^2+\sigma\parallel v^s+(a+\xi)\omega\|^2+m|\eta^s+(a+L)\omega|^2+\frac{I_h}{2}|\omega|^2$$

The symmetric motions are extracted from the model (25) as

$$\frac{d}{dt}z^s(t)=\mathcal{A}^s z^s(t)+\mathcal{B}^s u^s(t) \tag{26}$$

where

$$\mathcal{A}^s=\begin{bmatrix}0&I&0&0\\A_{21}&0&0&0\\A_{31}&0&0&0\\A_{41}&0&0&0\end{bmatrix}, \qquad \mathcal{B}^s=\begin{bmatrix}0&0\\-\frac{(a+\xi)}{I_h}&0\\-\frac{(a+L)}{I_h}&\frac{1}{m}\\1/I_h&0\end{bmatrix}, \qquad u^s(t)=\begin{bmatrix}M(t)\\T^s(t)\end{bmatrix} \tag{27}$$

and

$$[A_{21}(w^s)](\xi)=-\frac{(EI)}{\sigma}w^s_{\xi\xi\xi\xi}(\xi)-2\frac{(EI)}{I_h}(a+\xi)b(w^s,a) \qquad A_{31}(w^s)=\frac{(EI)}{m}w^s_{\xi\xi\xi}(L)-2\frac{(EI)}{I_h}(a+L)b(w^s,a)$$

$$A_{41}(w^s)=2\frac{(EI)}{I_h}b(w^s,a)$$

The domain of the symmetric state generator $\mathcal{A}^s$ is

$$D(\mathcal{A}^s)=\left\{z\in\mathcal{H}^s\,\middle|\, \begin{array}{c} w^s\in H^4, \qquad v^s\in H^2_0\\ w^s(0)=w^s_\xi(0)=w^s_{\xi\xi}(L)=0, \qquad v^s(0)=v^s_\xi(0)=v^s_{\xi\xi}(L)=0, \qquad v^s(L)=\eta\end{array}\right\}$$

The weak form of Eq. (26) is

$$\left\langle \frac{d}{dt} z^s(t), \Psi \right\rangle_{\mathcal{H}^s} = \langle \mathcal{A}^s z^s(t), \Psi \rangle_{\mathcal{H}^s} + \langle \mathcal{B}^s u^s(t), \Psi \rangle_{\mathcal{H}^s}$$

where $\Psi = \mathrm{col}(\Psi^w, \Psi^v, \Psi^\eta, \Psi^\omega)$. Using the inner product, this expands to

$$\left\langle \frac{d}{dt} z^s(t), \Psi \right\rangle_{\mathcal{H}^s} = \frac{d}{dt}\Bigg[(EI) \int_0^L w^s_{\xi\xi}(t,\xi) \Psi^w_{\xi\xi}(\xi)\, d\xi + \sigma\Bigg(\int_0^L [v^s(t,\xi) + (a+\xi)\omega(t)][\Psi^v(\xi) + (a+\xi)\Psi^\omega]\, d\xi + m[\eta^s(t) + (a+L)\omega(t)][\Psi^\eta + (a+L)\Psi^\omega] + \frac{I_h}{2}\omega(t)\Psi^\omega \Bigg)\Bigg]$$

$$= \frac{d}{dt}\Bigg[(EI) \int_0^L w^s_{\xi\xi}(t,\xi) \Psi^w_{\xi\xi}(\xi)\, d\xi + \sigma\Bigg(\int_0^L v^s(t,\xi)\Psi^v(\xi)\, d\xi + \int_0^L v^s(t,\xi)(a+\xi)\, d\xi \Psi^\omega + \int_0^L (a+\xi)\Psi^v(\xi) d\xi \omega(t) + \frac{(a+\xi)^3}{3}\Big|_0^L \omega(t)\Psi^\omega \Bigg) + \frac{I_h}{2}\omega(t)\Psi^\omega \Bigg] \tag{28}$$

For the right-hand side we have

$$\langle \mathcal{A}^s z^s, \Psi \rangle_{\mathcal{H}^s} = \left\langle \begin{bmatrix} v^s \\ A_{21}(w^s) \\ A_{31}(w^s) \\ A_{41}(w^s) \end{bmatrix}, \begin{bmatrix} \Psi^w \\ \Psi^v \\ \Psi^\eta \\ \Psi^\omega \end{bmatrix} \right\rangle_{\mathcal{H}^s} = (EI) \int_0^L v^s_{\xi\xi} \Psi^w_{\xi\xi}\, d\xi \tag{28a}$$

$$+ \sigma \int_0^L [A_{21}(w^s) + (a+\xi)A_{41}w^s][\Psi^v + (a+\xi)\Psi^\omega]\, d\xi \tag{28b}$$

$$+ m[A_{31}(w^s) + (a+L)A_{41}w^s][\Psi^\eta + (a+L)\Psi^\omega] \tag{28c}$$

$$+ \frac{I_h \Psi^\omega}{2} A_{41}(w^s) \tag{28d}$$

Expression (28b) evaluates to

$$-(EI)\Bigg(\int_0^L w^s_{\xi\xi}\Psi^v_{\xi\xi}\, d\xi + w^s_{\xi\xi\xi}(L)\Psi^v(L) + [(a+L)w^s_{\xi\xi\xi}(L) + b(w^s, a)]\Psi^\omega \Bigg)$$

whereas Expression (28c) becomes

$$(EI) w^s_{\xi\xi\xi}(L)[\Psi^\eta + (a+L)\Psi^\omega]$$

and Expression (28d) is given by

$$(EI)\Psi^\omega b(w^s, a)$$

Combining these, we find

$$\langle \mathcal{A}^s z^s, \Psi \rangle_{\mathcal{H}^s} = (EI)\Bigg(\int_0^L v^s_{\xi\xi}\Psi^w_{\xi\xi}\, d\xi - \int_0^L w^s_{\xi\xi}\Psi^v_{\xi\xi}\, d\xi \Bigg) \tag{29}$$

Note in particular that $\langle \mathcal{A}^s z^s, z^s \rangle_{\mathcal{H}^s} = 0$ [cf. Eq. (17)], so that $\mathcal{A}^s$ is dissipative (in fact, conservative).

Lastly, the control terms are

$$\langle \mathcal{B}^s u^s, \Psi \rangle_{\mathcal{H}^s} = \frac{\Psi^\omega}{2} u^s_1 + [\Psi^\eta + (a+L)\Psi^\omega] u^s_2 \tag{30}$$

Note that in constructing the weak form, the state-space structure dictated the form of the inner product, including boundary terms arising from the ODE part of the model [e.g., the Ψ^η and Ψ^ω terms in Expression (28) and Eqs. (29) and (30)].

VI. Galerkin Approximation

We use cubic spline functions for the state components w and v to construct a finite-dimensional approximation for the state-space $\mathcal{H}^s$. More specifically, for integer $N > 3$ we impose a uniform grid $\mathcal{G}^N = \{\xi_j = j\frac{L}{N} | j = 0, 1, \ldots, N\}$, and consider linear combinations of the usual $N+3$ cubic-splines that satisfy the homogeneous boundary conditions $b_j(0) = b_j'(0) = b_j''(L) = 0$, $j = 1, 2, \ldots, N$. A typical set of spline functions is shown in Fig. 2.

Using these spline functions, we construct basis vectors $\boldsymbol{b}_j \in \mathcal{H}^s$

$$\boldsymbol{b}^N_k = \begin{bmatrix} b^N_k(\xi) \\ 0 \\ 0 \\ 0 \end{bmatrix}, \qquad \boldsymbol{b}^N_{N+k} = \begin{bmatrix} 0 \\ b^N_k(\xi) \\ b^N_k(L) \\ 0 \end{bmatrix} \in \mathcal{H}^s$$

$$k = 1, \ldots, N, \qquad \boldsymbol{b}^N_{2N+1} = \begin{bmatrix} 0 \\ 0 \\ 0 \\ 1 \end{bmatrix}$$

and seek a solution

$$z^s(t) \approx \sum_{j=1}^{2N+1} z^N_j(t) \boldsymbol{b}^N_j \tag{31}$$

The form of Eq. (31) is used in the weak form; the basis vectors $\boldsymbol{b}_i$ are also used for the test functions Ψ and the result is the finite-dimensional system

$$M^N \dot{z}^N(t) = H^N z^N(t) + B^N u^s(t) \tag{32}$$

The $(2N+1) \times (2N+1)$ matrix M^N is given by

$$M^N \triangleq \langle \boldsymbol{b}^N_j, \boldsymbol{b}^N_i \rangle_{\mathcal{H}^s} = \begin{pmatrix} (EI)\int b_j'' b_i'' & 0 & 0 \\ 0 & \langle b_j, b_i \rangle_\sigma & \langle (a+\xi), b_i \rangle_\sigma \\ 0 & \langle b_j, (a+\xi) \rangle_\sigma & \langle (a+\xi), (a+\xi) \rangle_\sigma + \frac{I_h}{2} \end{pmatrix} \tag{33}$$

where

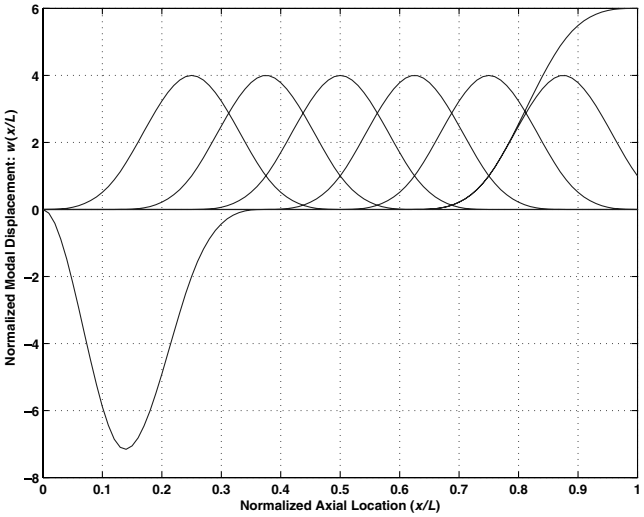

Fig. 2 Cubic spline functions for $N = 8$.

Table 3 Modal frequencies

Mode	Ω, Hz
1	0.264
2	0.855
3	1.780
4	3.047
5	4.676
6	6.725
7	9.232
8	12.081

$$\langle f, g\rangle_\sigma \triangleq \sigma \int_0^L f(\xi)g(\xi)\,\mathrm{d}\xi + mf(L)g(L)$$

The lower right element is the moment of inertia of (half) the system shown in Fig. 1 (i.e., a single beam with tip-mass plus one-half the hub-inertia). Furthermore, the $(2N+1)\times(2N+1)$ matrix H^N is given by

$$H^N \triangleq \langle \mathcal{A}^s \boldsymbol{b}_j^N, \boldsymbol{b}_i^N\rangle_{\mathcal{H}^s} = \begin{pmatrix} 0 & (EI)\int b_j'' b_i'' & 0 \\ -(EI)\int b_j'' b_i'' & 0 & 0 \\ 0 & 0 & 0 \end{pmatrix} \quad (34)$$

whereas the $(2N+1)\times 2$ control matrix is

$$B^N \triangleq \langle \mathcal{B}^{(j)}, \boldsymbol{b}_i^N\rangle_{\mathcal{H}^s} = \begin{pmatrix} 0 & 0 \\ 0 & b_i(L) \\ \frac{1}{2} & (a+L) \end{pmatrix} \quad (35)$$

Note, we have suppressed N-dependence on the RHS in Eqs. (33–35).

The state-space formulation provides a framework for convergence of the approximations, that is $z^N \to z^s$. More specifically, given an initial state $z_o \in \mathcal{H}^s$, and given a control u^s: $[0,T] \mapsto \mathbb{R}^2$, we have [[14], see the Trotter–Kato Theorem, page 87 and the following pages (*ff*)]

$$\lim_{N\uparrow\infty} \left\| z^s(t) - \sum_{j=1}^{2N+1} z_j^N(t)\boldsymbol{b}_j^N \right\|_{\mathcal{H}^s} = 0 \qquad \text{(uniformly in } t\text{)}$$

From briefing notes,[§¶] $I_o \approx 28\times 10^6$ kg/m^2, including a hub-inertia of 6000 kg/m^2; the mass of a single 150 m beam truss, including radar panels, is about 1780 kg; the stiffness parameter $EI/L \approx 75.1\times 10^6$ N · m. We estimate the mass of the tip-thruster as 10 kg, and the hub radius as 2 m. Modal frequencies for the nominal system are reported in Table 3.

VII. Minimum Angular Momentum

We now turn to the problem of making efficient use of the stored angular momentum. Although devices, such as gas thrusters or magnetic torquers may ultimately be practical in the ISAT application, the initial concept is that control torque for slewing maneuvers will be provided by a collection of control-moment gyros and momentum wheels. Thus, tip-thrust T^s is not used, so that only the first column of the operator $\mathcal{B}^s$ in Eq. (27) is used. Because there are limits on the available angular momentum, we are led to consider the following problem:

Problem $\mathcal{P}1$: Given the system data and parameters $\theta_f, t_f > 0$, find u^*: $[0,t_f] \mapsto \mathbb{R}$ to transfer the system (26) from $z^s(0) = 0$ to $z^s(t_f) = 0$, with

$$\int_0^{t_f} z_4^s(t)\,\mathrm{d}t = \theta_f$$

while minimizing

$$J = \int_0^{t_f} |u(t)|\,\mathrm{d}t$$

Note that problem $\mathcal{P}1$ seeks to minimize the control angular momentum, but does not impose a bound on the instantaneous control (torque). It is useful first to consider the case of a rigid spacecraft.

One expects that an optimal maneuver will consist of a *spin-up* phase, (possibly) a *coasting* phase and, finally, a *stopping* phase. Simple momentum conservation suggests that equal momentum (magnitude) be used in the two active phases (say, h) and that the maximum possible angular rate during the coasting phase is h/I_o.

Problem $\mathcal{P}1$ is not well-stated because it does not clearly specify the class of control functions u^*: $[0,t_f] \mapsto \mathbb{R}$ admitted to the competition. It is possible to formulate the problem in the class of *impulse controllers* [[16], see pages 324 *ff*]. In this setting, it can be shown that the optimal control for the rigid body (alone) is a starting impulse at $t=0$, a coasting arc with zero control, and a stopping impulse at $t=t_f$. Intuitively, we reason that by impulsively starting the rotation at $t=0$ (and stopping it at $t=t_f$) one is able to have the system rotate at maximum angular rate for the entire time. Any smooth buildup of rotation rate takes longer to accomplish the rotation. Here again, simple analysis for the rigid-body case reveals that the minimum angular momentum required is related to the problem parameters by

$$h_{\min} = \frac{I_o\theta_f}{t_f} \quad (36)$$

Representative results for ISAT are given in Table 4. Comparing Eq. (36) with the discussion at the end of Sec. I, we can see that for the rigid body alone, the minimum-effort control requires a 1.5 times the minimum angular momentum, whereas the minimum-time control requires twice as much.

Table 4 Minimum-momentum maneuvers, rigid-body, $\theta_f = \pi/2$

Time, min	Angular momentum, N · m/s
15	4.89×10^4
30	2.44×10^4
60	1.22×10^4
90	0.81×10^4

Of course, truly impulsive control cannot be realized in practice, and would probably not be desirable for a flexible structure in any case. Hence, we shall restrict the class of controls in problem $\mathcal{P}1$.

A. Versine Family of Inputs

Fundamentally, we are interested in a family of smooth functions that are (or can be) *impulselike* near $t=0^+$ and $t=t_f^-$. An interesting class of such input functions[§] is given by

$$u(t;\tilde{M},T_1,T_2) = \begin{cases} \tilde{M}/2[1-\cos(2\pi t/T_1)] & 0 \le t < T_1 \\ 0 & T_1 \le t \le T_1+T_2 \\ -\tilde{M}/2[1-\cos(2\pi/T_1)(t-T_1-T_2)] & T_1+T_2 \le t < 2T_1+T_2 \end{cases} \quad (37)$$

T_1 is the period of the versine function [versine$(\sigma) = 1-\cos(\sigma)$], T_2 is a coasting interval (see Fig. 3), and $\tilde{M}$ is the peak value of the applied moment. Input functions in this three-parameter family are continuously differentiable ($C^1[0,t_f]$), and we have

$$h \triangleq \int_0^{T_1} |u(t;\tilde{M},T_1,T_2)|\,\mathrm{d}t = \frac{\tilde{M}T_1}{2}$$

From this, and from Fig. 3, one can see that if we let $\tilde{M} \uparrow \infty$, and $T_1 \downarrow 0$ while maintaining $\tilde{M}T_1/2 = h$ (constant), an impulsive

¶T. Murphey, briefing slides & personal communications, Nov. & Dec. 2004.

control is realized. Control histories similar to those in Fig. 3 were developed in [5] for minimum-fuel (thruster) rotational maneuvers.

We are interested in the modal response to this input; that is, in initial-value problems of the form

$$\ddot{\zeta}_i(t) + \Omega_i^2 \zeta_i(t) = g_i u(t), \qquad \dot{\zeta}_i(0) = \zeta_i(0) = 0$$

For the rigid-body mode ($\Omega_1 = 0$) we find

$$\frac{\zeta_1(t;\tilde{M},T_1,T_2)}{\tilde{M}g_1/2} = \begin{cases} \frac{t^2}{2} + \frac{1}{\tilde{\omega}^2}(\cos\tilde{\omega}t - 1) & 0 \le t < T_1 \\ \cdots & \cdots \\ T_1\left[t - \frac{T_1}{2}\right] & T_1 \le t \le T_1 + T_2 \\ \cdots & \cdots \\ \frac{1}{\tilde{\omega}^2}[1 - \cos\tilde{\omega}(t - T_1 - T_2)] + T_1\left[t - \frac{T_2}{2}\right] - \frac{1}{2}(t - T_1 - T_2)^2 & T_1 + T_2 \le t < 2T_1 + T_2 \\ \cdots & \cdots \\ T_1(T_1 + T_2) & 2T_1 + T_2 \le t < \infty \end{cases} \tag{38}$$

Here, we have used $\tilde{\omega} \triangleq 2\pi/T_1$. A normalized displacement response for the rigid-body mode is shown in Fig. 4. Note that for $t > 2T_1 + T_2$, $\zeta_1(t)$ remains constant at the value $\zeta_1(2T_1 + T_2) = (g_1\tilde{M}/2)T_1(T_1 + T_2)$. Problem $\mathcal{P}1$ restricted to rigid-body motions and to the class of controls (37) is

Problem $\mathcal{P}2$: Given the system data I_o and parameters $\theta_f, t_f > 0$, find (nonnegative) parameters $\tilde{M}, T_1, T_2 < \infty$, so that $u(t;\tilde{M},T_1,T_2)$: $[0,t_f] \mapsto \mathbb{R}$ transfers the system (5) from $\theta(0) = \dot{\theta}(0) = 0$ to $\theta(t_f) = \theta_f$, $\dot{\theta}(t_f) = 0$, while minimizing

$$\int_0^{T_1} |u(t)|\,\mathrm{d}t$$

In dimensional variables we have

$$t_f = 2T_1 + T_2 \qquad \theta_f = \frac{\tilde{M}}{2I_o}T_1(T_1 + T_2) \qquad h = \frac{\tilde{M}T_1}{2} \tag{39}$$

The first two equations can be used to eliminate $\tilde{M}$ and T_2, leading to

$$h = \frac{I_o\theta_f}{(t_f - T_1)}, \qquad 0 < T_1 \le \frac{t_f}{2} \tag{40}$$

which is to be minimized by choice of T_1. Clearly, h decreases as $T_1 \downarrow 0$, but the choice $T_1 = 0$ is not admissible because it requires unbounded (impulsive) control torque ($\tilde{M} = 2h/T_1$).

Because problem $\mathcal{P}2$ does not have a solution, our formulation requires further modification. Figure 5 shows results for minimum angular momentum over a range of maneuver times for three values of a bound on the applied moment ($|M(t)| \le \tilde{M}$). The left end of each curve reaches a vertical asymptote; that is, there is a lower bound on maneuver time. These curves can be interpreted as feasibility boundaries: it is not possible, using controls from the class (37) with $|M(t)| \le \tilde{M}$, to achieve time/angular momentum values to the left or below. For example, with $|M(t)| \le 300$ N · m and $h \le 20,000$ N · m/s, the minimum maneuver time is about 40 min. Recall that in the minimum-time problem (see Table 1) with control torque bound $\tilde{M} = 300$ N · m, the maneuver was accomplished in about 13 min, but with a much larger expenditure of momentum (about 115,000 N · m/s). Similarly, the minimum-effort formulation (see Table 2) with a bound of 300 N · m accomplishes the maneuver in a little under 16 min but requires more than 70,000 N · m/s of stored momentum.

B. Flexible Mode Response

Next, we consider the response of a flexible structure to versine control inputs. For the flexible modes ($i = 2, \ldots,$ $\Omega_i > \Omega_{i-1}$)

$$\frac{\zeta_i(t;\Omega_i,\tilde{M},T_1,T_2)}{\tilde{M}g_i/2} = \begin{cases} \frac{1}{\Omega_i^2}(1 - \cos\Omega_i t) + \frac{1}{\Omega_i^2 - \tilde{\omega}^2}(\cos\Omega_i t - \cos\tilde{\omega}t) & 0 \le t < T_1 \\ \cdots & \cdots \\ \left(\frac{1}{\Omega_i^2 - \tilde{\omega}^2} - \frac{1}{\Omega_i^2}\right)[\cos\Omega_i t - \cos\Omega_i(t - T_1)] & T_1 \le t \le T_1 + T_2 \\ \cdots & \cdots \\ -\frac{1}{\Omega_i^2} + \frac{1}{\Omega_i^2 - \tilde{\omega}^2}\cos\tilde{\omega}(t - T_1 - T_2) + \left(\frac{1}{\Omega_i^2 - \tilde{\omega}^2} - \frac{1}{\Omega_i^2}\right)[\cos\Omega_i t - \cos\Omega_i(t - T_1) - \cos\Omega_i(t - T_1 - T_2)] & T_1 + T_2 \le t < 2T_1 + T_2 \\ \cdots & \cdots \\ \left(\frac{1}{\Omega_i^2 - \tilde{\omega}^2} - \frac{1}{\Omega_i^2}\right)[\cos\Omega_i t - \cos\Omega_i(t - T_1) - \cos\Omega_i(t - T_1 - T_2) + \cos\Omega_i(t - 2T_1 - T_2)] & 2T_1 + T_2 \le t < \infty \end{cases} \tag{41}$$

We have assumed that $\tilde{\omega} \ne \Omega_i$. A typical displacement response for a flexible mode is shown in Fig. 6. Note that all of the terms in the expressions for the forced flexible response include a factor with Ω_i^2 in the denominator. In particular, the postmaneuver response includes the factor

$$\left(\frac{1}{\Omega_i^2 - \tilde{\omega}^2} - \frac{1}{\Omega_i^2}\right) = \frac{1}{\Omega_i^2}\underbrace{\left[\frac{1}{(\frac{\Omega_i}{\tilde{\omega}})^2 - 1}\right]}_{F_1(\frac{\Omega_i}{\tilde{\omega}})} = \frac{1}{\tilde{\omega}^2}\underbrace{\left[\frac{1}{(\frac{\Omega_i}{\tilde{\omega}})^2[(\frac{\Omega_i}{\tilde{\omega}})^2 - 1]}\right]}_{F_2(\frac{\Omega_i}{\tilde{\omega}})}$$

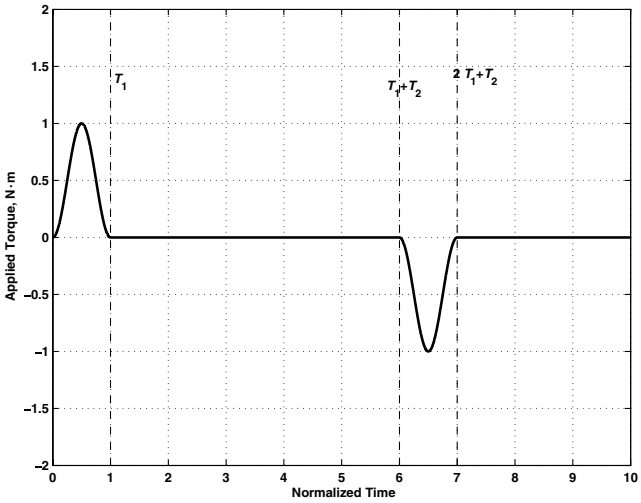

Fig. 3 Versine control torque, $\tilde{M} = 1$.

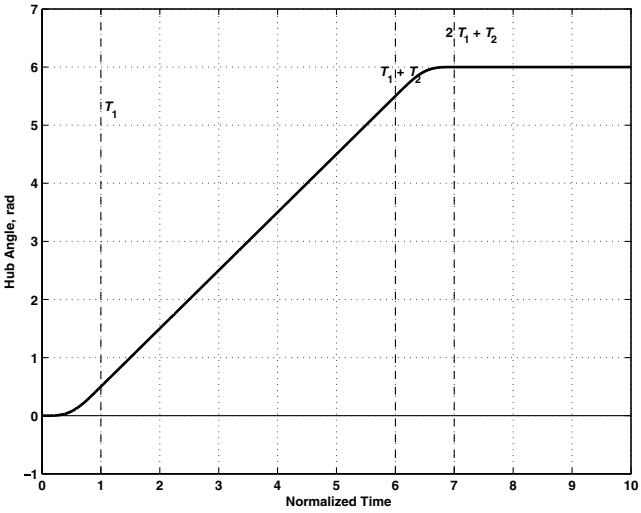

Fig. 4 Versine rigid-body displacement.

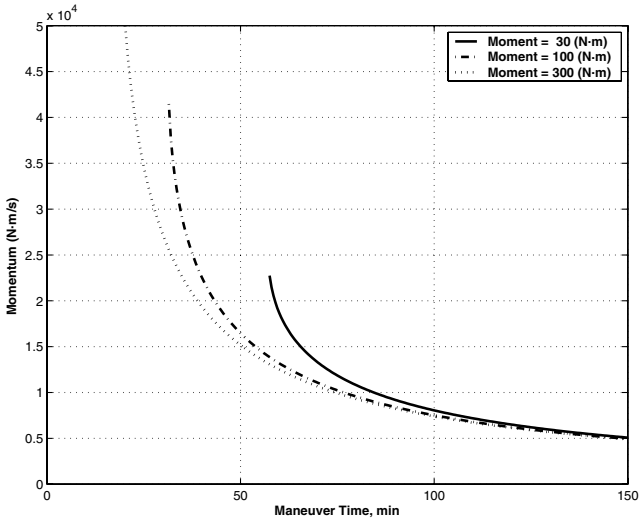

Fig. 5 Maneuver time/momentum trade; three moment values, $\theta_f = \pi/2$.

Thus, for fixed modal frequency Ω_1, as one varies the versine frequency ($\tilde{\omega} = 2\pi/T_1$), the postmaneuver displacement amplitude is described, in part, by the function $F_1(\Omega_1/\tilde{\omega})$. Similarly, for fixed versine frequency $\tilde{\omega}$, as one varies the modal frequency Ω_1, the

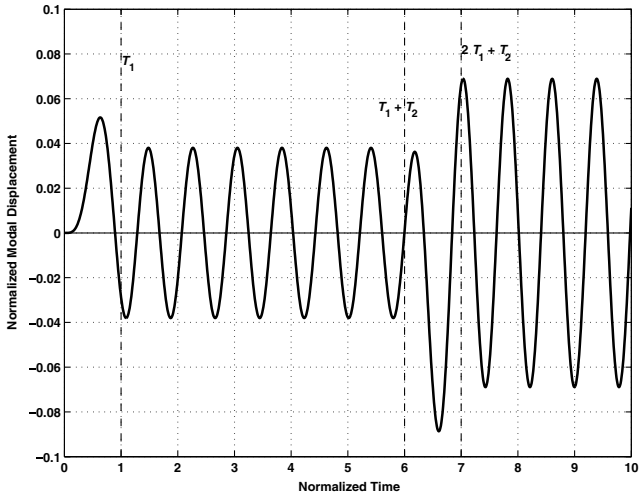

Fig. 6 Versine flexible mode displacement, $\Omega = 8$.

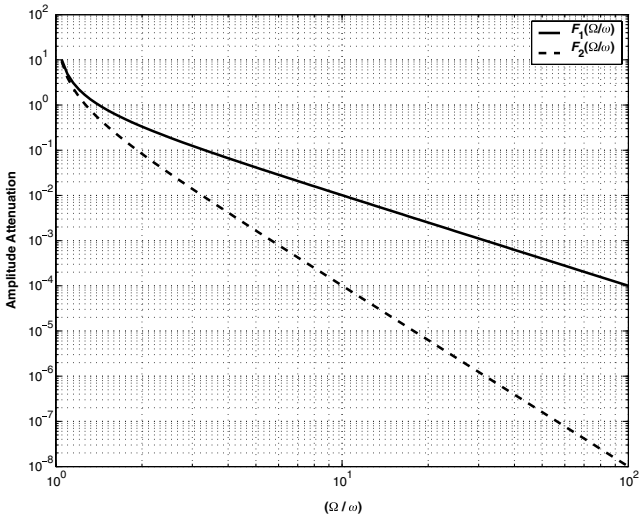

Fig. 7 Versine flexible mode amplitude attenuation.

postmaneuver displacement amplitude is described, in part, by the function $F_2(\Omega_1/\tilde{\omega})$. Graphs of these functions are shown in Fig. 7. Clearly, these functions decrease monotonically, so that larger values of $(\Omega_1/\tilde{\omega})$ are preferable.

It is worth noting that for the spin-up interval (i.e., $0 \le t < T_1$), the modal amplitude expression (41) can be written

$$\frac{\zeta_1(t;\Omega_1,a,T_1,T_2)}{ag_1/2} = \frac{1}{\Omega_1^2}\left(1 - \frac{\Omega_1^2}{\Omega_1^2 - \tilde{\omega}^2}\cos\tilde{\omega}t\right) + F_1(\Omega_1/\tilde{\omega})\frac{\cos\Omega_1 t}{\Omega_1^2}$$

which for large $(\Omega_1/\tilde{\omega})$ is approximated by the quasi-static response

$$\frac{\zeta_1(t;\Omega_1,a,T_1,T_2)}{ag_1/2} \approx \frac{1}{\Omega_1^2}(1 - \cos\tilde{\omega}t) \tag{42}$$

Expressions of the form

$$\sum_J a_j \cos(\Omega t - \phi_j)$$

in Eq. (41) can be combined to an amplitude/phase form. In particular, we have

$$\sum_J a_j \cos(\Omega t - \phi_j) = C\cos(\Omega t - \Phi)$$

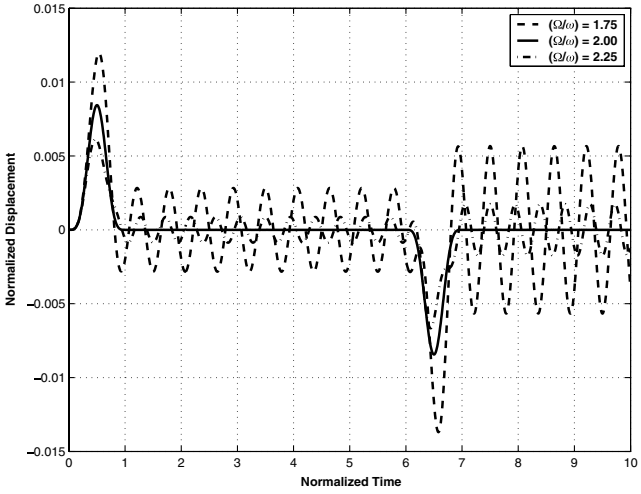

Fig. 8 Versine flexible mode comparison ($T_1 = 1, T_2 = 5$).

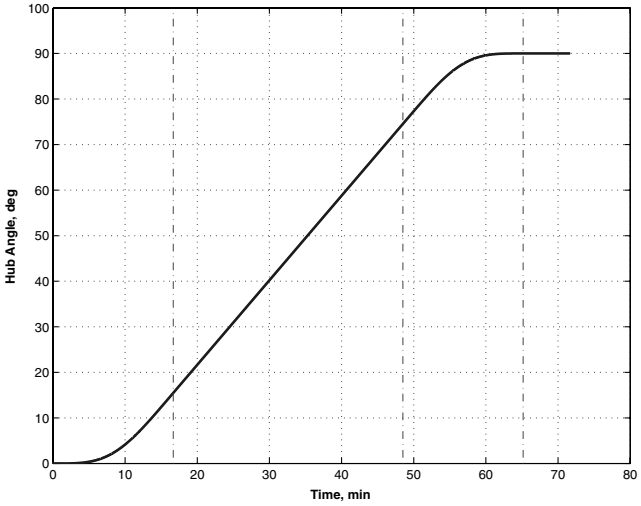

Fig. 9 Hub response with $M = 30$ N · m, $h = 15,000$ N · m/s.

where

$$C = \sqrt{\left(\sum_j a_j \cos\phi_j\right)^2 + \left(\sum_j a_j \sin\phi_j\right)^2}$$

$$\tan\Phi = \frac{\sum_j a_j \sin\phi_j}{\sum_j a_j \cos\phi_j}$$

On the coasting interval $[T_1, T_1 + T_2]$ this leads to $C = \sqrt{2(1 - \cos\Omega_1 T_1)}$, so that by choosing $\tilde{\omega} = \Omega_1/k$, for integer $k > 1$, the amplitude vanishes and the modal response on the coasting interval is identically zero. A more tedious calculation for the postmaneuver interval leads to

$$C = 4[1 - \cos(\Omega_1 T_1)] + 2[1 - \cos(2\Omega_1 T_1)]\cos(\Omega_1 T_2) + 2\sin(2\Omega_1 T_1)\sin(\Omega T_2)$$

Again, the choice $\tilde{\omega} = \Omega_1/k$ for integer $k > 1$ leads to vanishing amplitude and the postmaneuver modal response is identically zero.

Perhaps additional insight into the flexible-mode response can be gleaned by comparing responses for several values of the modal frequency Ω_1. Shown in Fig. 8 are responses for three values of the ratio $\Omega_1/\tilde{\omega}$. It appears that on the intervals with nonzero torque (i.e., $0 < t < T_1$ and $T_1 + T_2 < t < 2T_1 + T_2$), the peak deflection monotonically decreases with increasing $\Omega_1/\tilde{\omega}$. On the coasting interval and postmaneuver there is no such monotone behavior. Also, note that as predicted, for $\Omega_1 = 2\tilde{\omega}$, the response is identically zero during the coast and postmaneuver intervals.

C. Quasi-Static Response

The observations about modal responses suggest that we consider the quasi-static response of the system (27). In particular, we seek the quasi-static deflection $w_q^s(t, \xi)$ as the unique solution to

$$\left(\frac{EI}{\sigma}\right) w_{\xi\xi\xi\xi}(\xi) + \left(\frac{a + \xi}{I_h}\right)\{EI[w_{\xi\xi}(0) - a w_{\xi\xi\xi}(0)] + M(t)\} = 0$$

$$w(0) = w_\xi(0) = w_{\xi\xi}(L) = w_{\xi\xi\xi}(L) = 0$$

which is valid for the case of central hub torque only (no tip-thrust, no tip-mass). It can be shown that

$$w_q^s(t, \xi) = M(t)[c_0 + c_1\xi + c_2\xi^2 + c_3\xi^3]\xi^2$$

where the c_j are appropriate constants. For this case, it turns out that

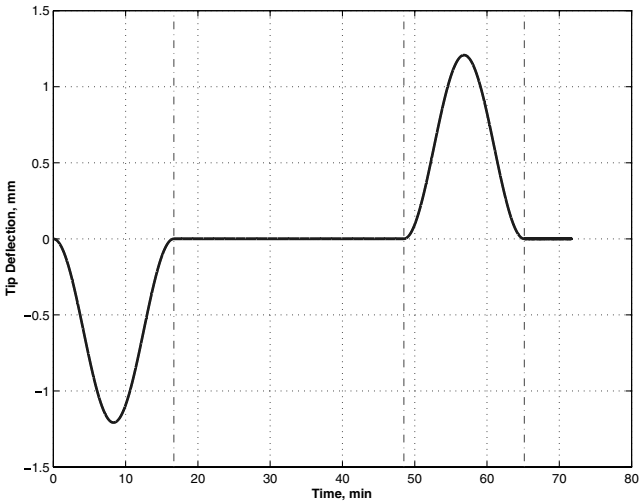

Fig. 10 Tip response with $M = 30$ N · m, $h = 15,000$ N · m/s.

$$\max_{0 \le \xi \le L} |w_q^s(t, \xi)| = |w_q^e(t, L)| = \underbrace{\frac{m_b L^4[11 + 15(a/L)]}{120 I_o(EI)}}_{\triangleq C_m} M(t) \quad (43)$$

Finally, we display the flexible structure response, modeled by the ODE system (31–35) with $N = 8$, to the versine control with a moment bound of 30 N · m, and a (spin-up) angular momentum budget of 15,000 N · m/s (i.e., $\tilde{M} = 30$ N · m, $T_1 = 1000$ s). Figure 9 shows the hub motion, whereas Fig. 10 shows the tip deflection. In this case, $(\Omega_1/\tilde{\omega}) \approx 250$ and it is clear that the response is well-approximated by the quasi-static result.

D. Minimum Momentum Versine Control: Quasi-Static Deflection Constraint

With some understanding of the effect of a bound on the applied torque, and of the flexible response to versine control, we pose the optimization problem:

Problem $\mathcal{P}3$: Given the system data and parameters θ_f, t_f, Δ, find (nonnegative) parameters $M, T_1, \tilde{T}_2 < \infty$, so that the control $u(t; \tilde{M}, T_1, T_2)$: $[0, t_f] \mapsto \mathbb{R}$ transfers the system (5) from $\theta(0) = \dot{\theta}(0) = 0$ to $\theta(t_f) = \theta_f$, $\dot{\theta}(t_f) = 0$ while minimizing

$$\int_0^{T_1} |u(t)|\, \mathrm{d}t$$

and satisfying

$$t_f = 2T_1 + T_2 \qquad \max_{0\le t\le t_f} |w_q^s(t, L)| \le \Delta$$

Here, $w_q^s(t, L)$ is the quasi-static tip-deflection history associated with the maneuver, and because of the inequality constraint, the problem is a *semi-infinite* optimization problem [17]. Note that the validity of the quasi-static approximation requires that $2\pi/T_1 = \tilde{\omega} \ll \Omega_1$. Comparing the deflection histories in Fig. 10 with the applied torque history in Fig. 3, it is apparent that the observed tip deflection is, indeed, linearly related to the (instantaneous) applied moment. It follows that a bound on the (quasi-static) tip displacement is equivalent to a bound on applied torque.

Problem $\mathcal{P}3$ has three design variables $(\tilde{M}, T1, T2)$. Because we seek to minimize $h = \tilde{M}T_1/2$, it is convenient to use variables (h, T_1, t_f) rather than $(\tilde{M}, T_1, T_2)$. From Eq. (40), the equality constraints on t_f and θ_f restrict the choice of variables to certain line segments in the (h, T_1) plane. Loci are shown as solid lines in Fig. 11 for $\theta_f = \pi/2$ and for several values of t_f. The right limit points on these curves are the points where $T_1 = t_f/2$ (and, hence $T_2 = 0$). Under the quasi-static approximation, the maximum deflection is proportional to the maximum applied moment, so that from Eq. (43) one has $\tilde{M} = \Delta/C_m$ Recalling Eq. (30), we get that

$$h = \frac{\Delta}{2C_m} T_1 \tag{44}$$

so that lines of specified maximum deflection are straight lines in the (h, T_1) plane. Several of these are shown as dashed lines in Fig. 11. Above and to the left of such lines, the maximum deflection exceeds the specified bound Δ. It is clear from the geometry in this figure that for specified (θ_f, t_f, Δ), the minimum momentum solution lies at the intersection of the specified t_f (solid) line and the specified Δ (dashed) line. In analytic terms, we have

$$T_1 = \frac{t_f}{2} - \hat{t} \quad \text{and} \quad T_2 = 2\hat{t}$$

where

$$\hat{t} = \sqrt{\left(\frac{t_f}{2}\right)^2 - \frac{2I_o\theta_f C_m}{\Delta}}$$

Clearly, if the specified time is too short $[t_f < 2\sqrt{2I_o\theta_f C_m/\Delta}]$, then the constraints are incompatible and the problem has no feasible points.

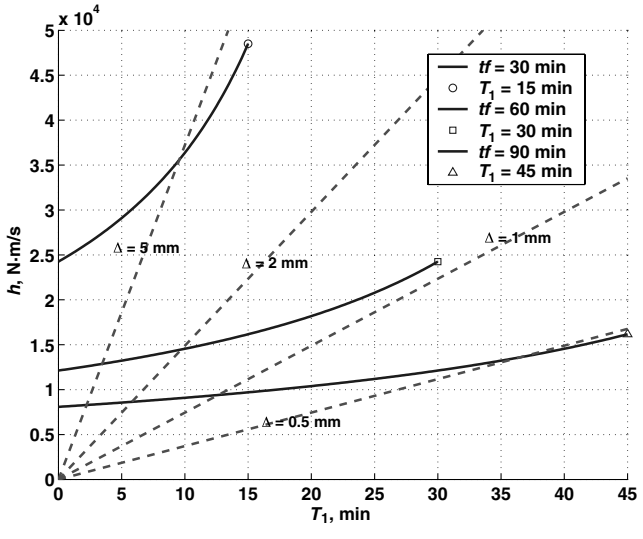

Fig. 11 Plane of h, T_1; constant t_f and constant Δ lines for $\theta_f = \pi/2$.

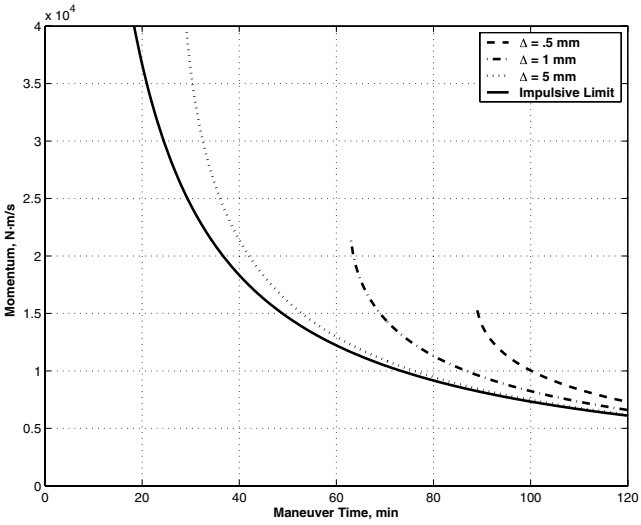

Fig. 12 Maneuver time/momentum trade for various deflection bounds, $\theta_f = \pi/2$.

Next, we solve a one-parameter family of problems $\mathcal{P}3$, with t_f as the parameter. Results of this calculation for several values of Δ are shown in Fig. 12. Notice that reducing the tip-deflection bound Δ, increases the required angular momentum for a given maneuver time. Additionally, as the tip-deflection bound Δ is decreased, the lower bound on maneuver time increases. For example, with $\Delta = 1$ mm, the least achievable maneuver time is about 62.5 min, and this requires a little under $16,500$ N · m/s of momentum for the spin-up maneuver (and an equal but opposite amount for stopping). The peak moment is about 24.8 N · m. For comparison, with $\Delta = 5$ mm, the least achievable maneuver time is about 28 min, requires a little over $52,000$ N · m/s of momentum for the spin-up maneuver, and the peak moment is about 124 N · m (this point is not in the range covered by the figure). For a specified maneuver time, one can read out the angular momentum required with a specified deflection bound. Table 5 gives required angular momentum for 70 and 100 min maneuvers with several tip-deflection bounds. Note that compared with the case with no active deflection bound ($\Delta = \infty$), the $\Delta =$ 5 mm bound can be achieved with little additional angular momentum.

E. Minimum Momentum Versine Control: Deflection Rate Constraints

The deflection constraint of problem $\mathcal{P}3$ arises from the observation that for the radar to function correctly, the positions of the active elements must be known within the specified tolerance Δ. Thus, if structural deflections are kept within this bound, the radar can operate successfully. The structural deformations constraint can be mitigated by introducing an active metrology/calibration system, which offers the possibility of measuring structural deflections. However, this metrology/calibration system will have a minimum update cycle time μ. Combining these ideas, T. Murphey [¶] has concluded that successful operation can be assured if the maximum deflection rate does not exceed Δ/μ. This motivates the following problem:

Problem $\mathcal{P}4$: Given the system data and parameters θ_f, t_f, V, find (nonnegative) parameters $\tilde{M}$, T_1, $T_2 < \infty$, so that the control

Table 5 Required momentum, $\theta_f = \pi/2$

Δ, mm	Momentum, N · m/s, $t_f = 70$ min	Momentum, N · m/s, $t_f = 100$ min
0.5	infeasible	9914
1	14,332	8171
5	10,844	7423
∞	10,393	7275

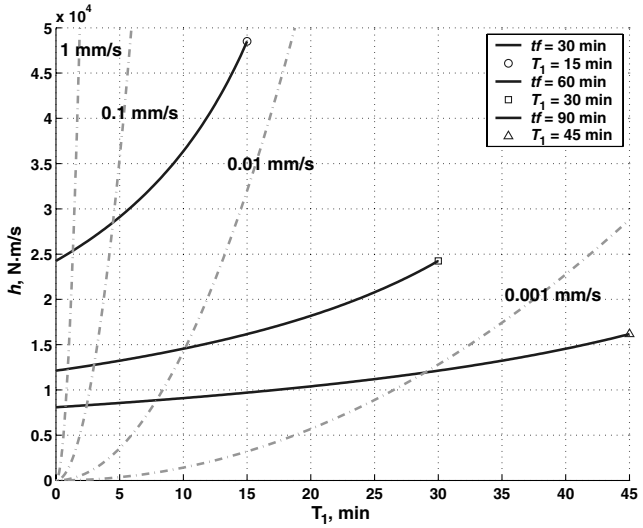

Fig. 13 Plane of h, T_1: constant t_f and constant V lines for $\theta_f = \pi/2$.

$u(t; \tilde{M}, T_1, T_2)$: $[0, t_f] \mapsto \mathbb{R}$ transfers the system (5) from $\theta(0) = \dot{\theta}(0) = 0$ to $\theta(t_f) = \theta_f$, $\dot{\theta}(t_f) = 0$, while minimizing

$$\int_0^{T_1} |u(t)| \, \mathrm{d}t$$

and satisfying

$$t_f = 2T_1 + T_2 \qquad \max_{0 \le t \le t_f} \max_{0 \le \xi \le L} |\dot{w}_q^s(t, \xi)| \le V$$

1. Quasi-Static Case

Our solution is predicated on the assumption that the deflection rate can be computed from the quasi-static formulation (43). That is, we compute the deflection rate from

$$\dot{w}_q^s(t, L) = C_m \dot{M}(t)$$

Using expression (37) for the applied moment, we find the peak deflection rate to be

$$\max_t |\dot{w}_q^s(t, L)| = C_m \frac{\tilde{M}}{2} \omega = \frac{\pi C_m \tilde{M}}{T_1} \tag{45}$$

The solid lines in Fig. 13 shows loci of feasible values in the (h, T_1) plane for $\theta_f = \pi/2$ and for several values of t_f. These are the same as the solid lines in Fig. 11. From Eq. (45) and the angular momentum expression, the deflection rate constraint is written as

$$h \le \frac{V}{2\pi C_m} T_1^2 \tag{46}$$

where the constant C_m has been defined in Eq. (43), and V is the upper bound on deflection rate in problem $\mathcal{P}4$. Equality in Eq. (46) defines a parabola in the (h, T_1) plane; admissible points are to the right and below this parabola. Figure 13 shows several constant deflection rate parabolas as dashed lines. From the figure, it appears that the $V = 0.1$ mm/s limit is not a stringent constraint; a great deal of the (h, T_1) plane is admissible. Increasing this limit moves the constraint closer to the h-axis. For specified θ_f and t_f, the minimum required angular momentum is achieved at the intersection of the specified θ_f and deflection rate (46) lines. Such points satisfy the cubic equation

$$T_1^3 - t_f T_1^2 + \underbrace{\frac{2\pi I_o \theta_f C_m}{V}}_{\triangleq C_T} = 0 \tag{47}$$

Table 6 Solutions to problem $\mathcal{P}5$, $\theta_f = \pi/2$, $V = 0.1$ mm/s

t_f, min	T_1, min	Momentum, N · m/s	Moment, N · m	Max deflection, mm
45	3.5	17,530	166	6.7
50	3.3	15,580	157	6.3
55	3.1	14,030	149	6.0
60	3.0	12,769	142	5.7
65	2.9	11,710	136	5.5
70	2.8	10,820	131	5.3
75	2.7	10,060	126	5.1
80	2.6	9400	122	4.9
85	2.5	8820	118	4.8
90	2.4	8310	115	4.6

Analysis of the cubic Eq. (47) shows that it will have one root on the interval $[0, t_f/2]$, if

$$t_f \ge 2\left(\frac{2\pi I_o \theta_f C_m}{V}\right)^{\frac{1}{3}}$$

Solutions to problem $\mathcal{P}4$ for $\theta_f = \pi/2$, $V = 0.1$ mm/s, and a range of values of t_f are shown in Table 6. In this case, the minimum feasible final time is a little under 16 min. We have not included the case $V = 10$ mm/s because the minimum h values require very low values of T_1, the spin-up maneuver time. At low values of T_1, the quasi-static deflection approximation will not be valid and this complicates application of the deflection rate constraint. Moreover, because the constant t_f lines in Fig. 13 are nearly horizontal as $T_1 \to 0^+$, the marginal saving in required angular momentum is quite small.

Note that if the maximum angular momentum available is 15,000 N · m/s, then the least maneuver time is about 51 min, and the maximum tip-deflection is a bit more than 6 mm.

2. Quasi-Static Case: Solution Sensitivity

Here, we briefly present an analysis of the sensitivity of the solution to problem $\mathcal{P}4$ to parameters. Of particular interest is the sensitivity to the beam stiffness parameter EI. We begin by rewriting Eq. (47) in a slightly more general form

$$T_1(q)^3 - t_f T_1(q)^2 + C_T(q) = 0$$

where q is some generic parameter in the expression for the C_T, and the notation indicates that the spin-up time T_1 implicitly depends on this parameter. We are particularly interested in the case $q = (EI)$. Differentiation leads to the sensitivity equation

$$\frac{\partial T_1}{\partial q} = \frac{\partial C_t / \partial q}{T_1(2t_f - 3T_1)}$$

With the spin-up sensitivity known, the sensitivity of the required spin-up angular momentum follows by differentiating Eq. (44)

$$\frac{\partial h}{\partial q} = -\frac{h}{(t_f - T_1)} \frac{\partial T_1}{\partial q}$$

Note that this expression would contain additional terms if the parameter q depended on I_o or θ_f. For the case $q \sim (EI)$, we find from Eqs. (43) and (47) that

$$\frac{\partial C_T}{\partial (EI)} = -\frac{C_T}{(EI)}$$

so that

$$\frac{\partial T_1}{\partial (EI)} = \frac{-C_T}{T_1(2t_f - 3T_1)} \frac{1}{(EI)} \quad \text{and}$$

$$\frac{1}{h} \frac{\partial h}{\partial (EI)} = \frac{-C_T}{T_1(t_f - T_1)(2t_f - 3T_1)} \frac{1}{(EI)}$$

From the latter of these, we see that the percentage change in required

Table 7 Sensitivities to stiffness, $\theta_f = \pi/2$, $V = 0.1$ mm/s

t_f, min	T_1-sensitivity	h-sensitivity	$\tilde{M}$-sensitivity	Δ_{tip}-sensitivity
45	−0.522	−0.044	0.566	−0.434
50	−0.518	−0.037	0.555	−0.445
55	−0.516	−0.031	0.547	−0.453
60	−0.513	−0.027	0.540	−0.460
65	−0.512	−0.024	0.535	−0.465
70	−0.510	−0.021	0.531	−0.469
75	−0.509	−0.019	0.528	−0.472
80	−0.508	−0.017	0.525	−0.475
85	−0.508	−0.015	0.523	−0.477
90	−0.507	−0.014	0.521	−0.479

angular momentum is the percentage change in stiffness multiplied by a factor; that is

$$\frac{\delta h/h}{\delta(EI)/(EI)} = \frac{-C_T}{T_1(t_f - T_1)(2t_f - 3T_1)} = \frac{-T_1}{(2t_f - 3T_1)} \tag{48}$$

Similar analyses shows that the percentage change in required peak moment is related to the percentage change in stiffness by the factor

$$\frac{\delta\tilde{M}/\tilde{M}}{\delta(EI)/(EI)} = \frac{t_f}{(2t_f - 3T_1)} \tag{49}$$

and that the change in peak tip-deflection is related to the percentage change in stiffness by the factor

$$\frac{\delta\Delta_{\text{tip}}/\Delta_{\text{tip}}}{\delta(EI)/(EI)} = \frac{-(t_f - 3T_1)}{(2t_f - 3T_1)} \tag{50}$$

Values for these factors are shown in Table 7. Note that for $t_f = 45$ min, the momentum sensitivity factor is approximately −0.044, indicating that *in linear approximation* a 10% increase in stiffness EI would engender about a 0.4% decrease in required angular momentum. Similarly, such an increase in stiffness would engender a 5.7% increase in maximum required moment and a 4.3% decrease in the maximum tip-deflection. For longer maneuver times, the momentum and moment sensitivities are reduced, whereas the tip-deflections sensitivity increases in absolute value. Recall that, in our quasi-static model, the stiffness parameter appears only through the constraint on deflection rate.

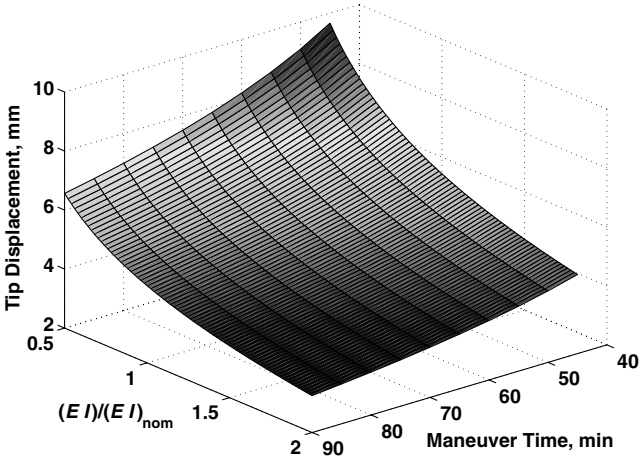

Fig. 15 Effects of (EI) and t_f variations on tip deflection, $\dot{\Delta}_{\text{tip}} = 0.1$ mm/s.

The results in Table 7 provide a linear estimate of the effects of changes from the nominal values of the stiffness parameter EI on the solution to problem $\mathcal{P}5$. Figure 14 displays the nonlinear variation of these parameters for the case $t_f = 45$ min. Consistent with the linearized results, we see that the effect on the required angular momentum h is modest; varying from 1.03 times the nominal for EI at one-half its nominal value, to 0.975 times the nominal for EI at twice its nominal value. Perhaps the most significant effect is on the maximum tip-deflection Δ_{tip}. With the nominal EI at one-half its nominal value, the tip-deflection is increased by more than 40%, whereas with the nominal EI at twice its nominal value, the tip-deflection is decreased by about 30%. Figure 15 surveys the effects of changes in stiffness EI and final time on the maximum tip-deflection. Note that all of these cases satisfy the deflection-rate constraint $\dot{\Delta}_{\text{tip}} \leq 0.1$ mm/s.

VIII. Conclusions

State-space formulation and semigroup theory afford useful tools to establish well-posedness and convergent numerical approxima-

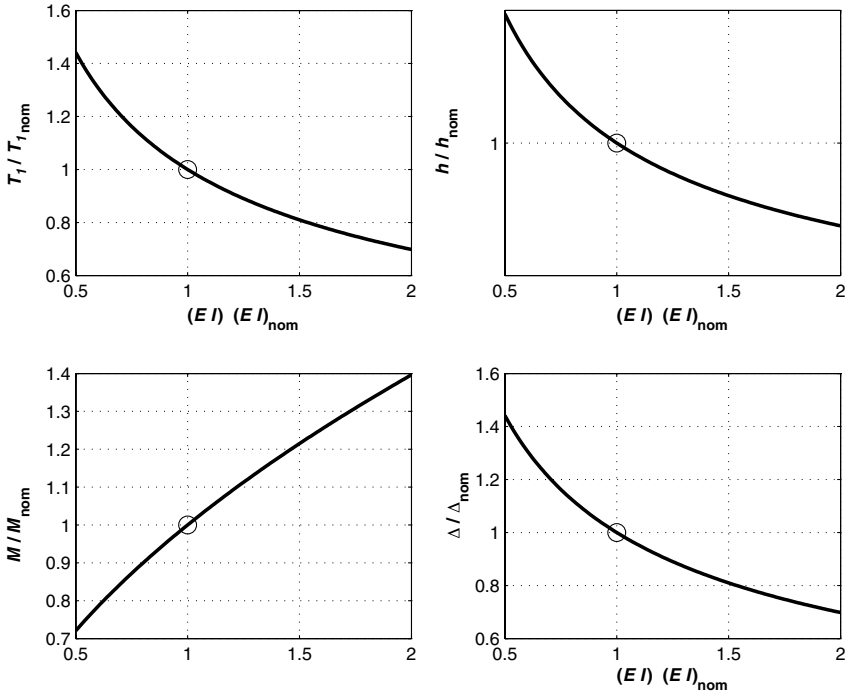

Fig. 14 Effects of (EI) variation on performance; problem $\mathcal{P}4$, $t_f = 45$ min.

tions for dynamic models that include PDEs. Because slewing of very large space structures requires judicious use of stored angular momentum, minimum momentum controls are of interest. However, care must be taken to ensure that the mathematical problem has a solution of practical interest. A versine family of control inputs provides a reasonable way to produce ISAT slewing maneuvers that are efficient in their use of time and momentum, yet allow for radar operations. Although other smooth approximations are possible, the versine leads to tractable closed-form characterization of the response. Quasi-static response approximations admit analytical treatment of the underlying optimization problem and provide useful insights for design tradeoffs. Sensitivity analyses are useful in design trades. For example, it was shown for the problem of minimizing angular momentum with a bound on deflection rate, that increasing structural stiffness EI decreases both the required momentum and the maximum deflection but increases the required moment.

Acknowledgments

This work was supported in part by Defense Advanced Research Projects Agency /Special Projects Office, NASA Langley Research Center, and the National Institute of Aerospace under grant VT-03-1, 2535, and in part by the Air Force Office of Scientific Research under grant F49620-03-1-0243. We are grateful to M. Mikulas (National Institute of Aerospace) and T. Murphey (Air Force Research Laboratory/Space Vehicles) for their helpful insights and comments.

References

[1] Ben-Asher, J. Z., "Time Optimal Slewing of a Flexible Spacecraft," Ph.D. Dissertation, Virginia Polytechnic Inst. and State Univ., Blacksburg, VA, June 1988.

[2] Ben-Asher, J. Z., "Optimal Slewing of Flexible Spacecraft with Prescribed Sensitivity of Terminal Control," AIAA Paper 1993-3771, Aug. 1993.

[3] Ben-Asher, J. Z., Burns, J. A., and Cliff, E. M., "Time Optimal Slewing of a Flexible Structure," *Journal of Guidance, Control, and Dynamics*, Vol. 15, No. 2, 1992, pp. 360–367.

[4] Byers, R. M., Vadali, S. R., and Junkins, J. L., "Near-Minimum Time, Closed-Loop Slewing of Flexible Spacecraft," *Journal of Guidance, Control, and Dynamics*, Vol. 13, No. 1, 1990, pp. 57–65.

[5] Carter, M. T., Vadali, S. R., and Singh, T., "Near Minimum-Time Maneuvers of Large Space Structures Using Parameter Optimization, AIAA Paper 1993-3714, Aug. 1993.

[6] Singh, G., Kabamba, P. T., and McClamroch, N. H., Planar, Time-Optimal, Rest-to-Rest Slewing Maneuvers of Flexible Spacecraft, *Journal of Guidance, Control, and Dynamics*, Vol. 12, No. 1, 1989, pp. 71–81.

[7] Singhose, W. E., Pao, L. Y., and Seering, W. P., "Slewing Multi-Mode Flexible Spacecraft Using Zero Derivative Robustness Constraints," *Journal of Guidance, Control, and Dynamics*, Vol. 20, No. 1, 1997, pp. 204–206.

[8] Thompson, R. C., Junkins, J. L., and Vadali, S. R., "Near Minimum-Time Open-Loop Slewing of Flexible Vehicles," *Journal of Guidance, Control, and Dynamics*, Vol. 12, No. 1, 1989, pp. 82–88.

[9] Vadali, S. R., Singh, T., and Carter, T., "Computation of Near-Minimum-Time Maneuvers of Flexible Spacecraft by Parameter Optimization," AIAA Paper 1992-4459, Aug. 1992.

[10] Neustadt, L. W., "Minimum Effort Control Systems," *SIAM Journal on Control and Optimization*, Vol. 1, No. 1, 1962, pp. 16–31.

[11] Juang, J., Turner, J. D., and Chun, H. M., "Closed-Form Solution for Feedback Control with Terminal Constraints," *Journal of Guidance, Control, and Dynamics*, Vol. 8, No. 1, 1984, pp. 39–43.

[12] Meirovitch, L., and Sharony, Y., "Accommodation of Kinematic Disturbances During Minimum-Time Maneuvers of Flexible Spacecraft," *Journal of Guidance, Control, and Dynamics*, Vol. 14, No. 2, 1991, pp. 241–250.

[13] Das, A., "Large Angle Maneuver Experiments in Ground-Based Laboratories," AIAA Paper 90-1236, 1990.

[14] Pazy, A., "Semigroups of Linear Operators and Applications to Partial Differential Equations," 2nd ed., Springer–Verlag, New York, 1983.

[15] Adams, R. A., *Sobolev Spaces*, Academic Press, New York, 1975.

[16] Lee, E. B., and Markus, L., "Foundations of Optimal Control Theory," Wiley, New York, 1967.

[17] Polak, E., "Optimization: Algorithms and Consistent Approximations," Springer, New York, 1997.